

Limitations of atomistic modeling to reveal ejection of proteins from charged nanodroplets

Victor Kwan, Pranav Ballaney, Titiksha, and Styliani Consta*

*Department of Chemistry, The University of Western Ontario, London, Ontario, Canada
N6A 5B7*

E-mail: sconstas@uwo.ca

Abstract

Molecular dynamics using atomistic modeling is frequently used to unravel the mechanisms of macroion release from electrosprayed droplets. However, atomistic modeling is currently feasible for only the smallest window of droplet sizes appearing at the end of a disintegrating droplet’s lifetime. The relevance of the observations made to the actual droplet evolution, which is much longer than the simulated sizes, has not been addressed. Here, we perform a systematic study of desolvation mechanisms of poly(ethylene glycol) (PEG), protonated peptides of different compositions and proteins in order to (a) examine whether atomistic modeling can establish the extrusion mechanism of proteins from droplets and (b) obtain insight for the charging mechanism in larger droplets than those simulated. Atomistic modeling of PEG charging shows that above a critical droplet size charging occurs transiently by transfer of ions from the solvent to the macroion, while below the critical size, the capture of the ion from PEG has a lifetime sufficiently long for extrusion of the charged PEG from an aqueous droplet. This is the first report of the role of droplet curvature in the conformations and charging of macroions. Simulations with highly hydrophobic peptides show that partial extrusion of a peptide from the droplet surface is rare relative to desolvation by drying-out. Differently from what has been presented in the literature we argue that atomistic simula-

tions have not sufficiently established extrusion mechanism of proteins from droplets and their charging mechanism. Moreover, we argue that release of highly charged proteins can occur at an earlier stage of a droplet’s lifetime than predicted by atomistic modeling. In this earlier stage, we emphasize the key role of jets emanating from a droplet at the point of charge-induced instability in the release of proteins.

Introduction

The chemical processes within ionization techniques, employed to transfer analyte species from the bulk solution into the gaseous phase for mass spectrometry (MS) analysis, have always been challenging to investigate. The question of “what is the mechanism by which a macroion obtains its charge?” appears with the first successes of the methods.^{12–27}

In spray-based ionization techniques that include sonic,²⁸ thermal,²⁹ and electrospray,^{12,30} droplets are the vehicles that transfer analytes from the bulk solution into the gaseous phase. Regardless of the spraying method, the droplets are charged and they are composed of solvent, which is often water, simple charge carriers such as H_3O^+ , Na^+ ions and the charged macroion. During their lifetime, they disintegrate via solvent evaporation and Coulomb fission events.

The droplet environment plays a decisive role in a macroion’s charge state. It is expected that competition between the dynamics of various processes such as solvent evaporation, proton

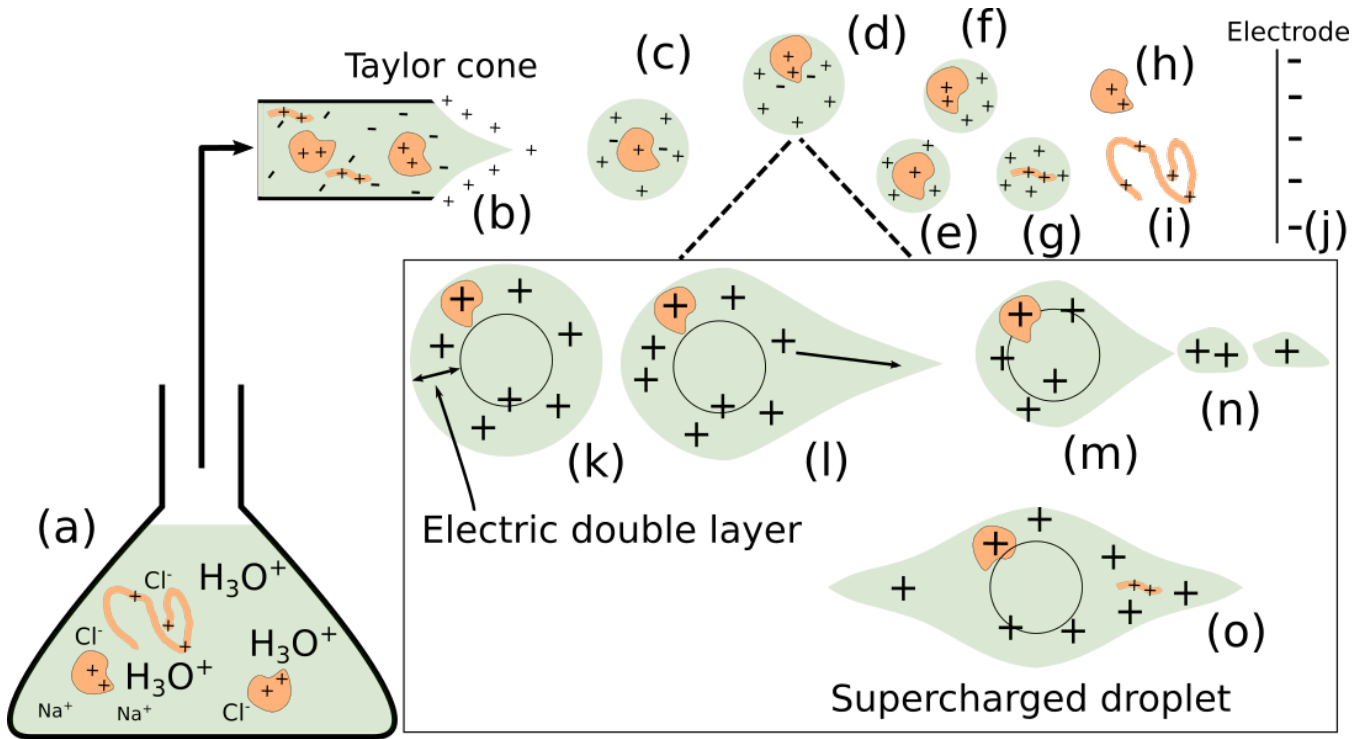


Figure 1: Schematic representation of transfer of macroions from the bulk solution to droplets to the gaseous phase in an electrospray process. Macroions are colored orange and can be compact or extended.¹ The “+” and “-” signs indicate charge carriers such as Na^+ , NH_4^+ , H_3O^+ for “+”, and CH_3COO^- , Cl^- for “-”. (a) Macroions in bulk solution that is to be sprayed. The ion distribution around them is described by Manning-Oosawa model.^{2,3} The solution is transferred to a capillary. (b) A Taylor cone^{4,5} at the tip of the capillary formed due to an applied external electric field. The polarity of the electric field can be positive or negative. In the schematic the electrospray is in the positive ion mode as indicated by the negative electrode in (j). (c)-(d) Nascent droplet aerosol originating from the Taylor cone. The droplets contain macroions, excess co-ions and counterions. The macroions can be found in different locations in the droplets. (e)-(g) Droplets travel along the electric field and shrink by undergoing a repeating cycle of solvent evaporation and Coulomb explosion events. (h)-(i) In the last stage desolvated macroions emerge. (j) Negative electrode that sets the polarity of the applied external electric field. (k)-(o) Details of a droplet’s division mechanism via jet formation.⁶ The circle within (k)-(o) indicates the inner boundary of the electric double layer.⁷⁻¹¹ In previous research⁹⁻¹¹ we estimated its thickness to be 1.5 nm-2.0 nm regardless of droplet size. Variations of external pressure along a droplet’s journey are not shown. Details are discussed in the text.

transfer reactions,^{31,32} Coulomb fission, possible conformational changes of macroions will determine a macroion’s charge state. Because of the multitude of processes that take place in a droplet’s lifetime, the precise mechanism via which macroions obtain their charge has not been settled yet. However, fundamental mechanisms have been proposed,^{8,14,15,33–35} which are analyzed in the next section.

Molecular dynamics (MD) using atomistic modeling is broadly used to reveal the macroion release mechanisms. However, atomistic modeling is limited to monitor disintegration of droplets comprised at most a couple of thousands of H₂O molecules, a protein and ions. This system size corresponds to an equimolar radius of several nanometers. In atomistic modeling it has been considered that macroion release occurs in this narrow window in a droplet’s lifetime without considering its long history. The problem is more severe at elevated temperature where non-equilibrium conditions are favored and thus, the droplet’s history plays a decisive role. Here, we addressed the feasibility of ejection mechanisms of macroions from charged aqueous nanodroplets using atomistic modeling. Poly(ethylene glycol) (PEG), protonated peptides of varying degree of hydrophobicity and myoglobin are selected as typical examples to demonstrate the likelihood of ejection. We also examine, how the insight obtained from the atomistic modeling of the smallest nanodroplets is transferable to droplets of larger size.

In order to provide the broader context of the problem and the limitations of the atomistic modeling in Fig. 1 we present a schematic of the entire aerolization process from the bulk solution to the release of macroions. In the bulk solution polyelectrolytes (macroions) (Fig. 1 (a)) are surrounded by a cloud of counterions, which affects their radius of gyration and conformation.^{2,3,36,37} The solution is injected to a capillary (Fig. 1 (b)) at the tip of which there is an external electric field. The application of the electric field induces a conical protrusion in the liquid surface that is called the Taylor cone^{4,5} shown in Fig. 1 (b). This is a critical step in the ionization process, where the liquid-

vapor interface of the cone accumulates ions of the same sign depending on the polarity of the applied electric field. The cone emits charged droplets as shown in Fig. 1 (c)-(d), where the charge carriers are the macroions and simple ions such as H₃O⁺, Na⁺, NH₄⁺ ions. Counterions such as Cl⁻, CH₃OO⁻ are also present in the nascent aerosol. The dimensions of the initially produced droplets depend on the specifics of the instrument and usually vary between a few hundreds of nanometers to micrometers. It is noted that in a huge ensemble of sprayed droplets a macroion can be statistically found anywhere in a droplet’s volume as shown in Fig. 1 (c)-(d). However, because of the prevalence of vapor-liquid interface, the likelihood for a macroion to be found on the surface is considerably higher than in the interior. It is believed that the macroions maintain the surrounding cloud of counterions as in the bulk solution.³⁸ Even though this assumption is reasonable, we think that it may break down because of the preference of macroions to be located in the outer layers of droplets where they may be affected by the electric double layer.^{9–11} This question is investigated in future work.

The sprayed droplets undergo a cycle of solvent evaporation and ion ejection events (Fig. 1 (c)-(g)), until the macroions (linear or compact) emerge (Fig. 1 (h)-(i)). For example, the droplets shown in Fig. 1 (c)-(d) may decrease in size by solvent evaporation. Once a droplet’s size reaches a critical point at which the electrostatic repulsive forces among excess ions of the same sign overcome the surface tension forces, the droplet divides. The point where these two forces are equal is called the Rayleigh limit^{39–43} (RL).

The RL is defined via the Rayleigh fissility parameter (X) given by

$$X = \frac{Q^2}{64\pi^2\gamma\epsilon_0 R^3} \quad (1)$$

where Q is the droplet charge, γ the surface tension, ϵ_0 and R are the permittivity of vacuum and the radius of the droplet, respectively. When $X = 1$, the charged droplet is at the RL. At $X < 1$ (“below” the RL) the droplet is sta-

ble wrt to small perturbations of its spherical shape. At $X > 1$ (“above” the RL) the droplet is unstable.

The mechanism by which a droplet emits ions is shown in Fig. 1 (k)-(o). The circle in Fig. 1 (k) indicates the presence of an electric double layer.⁷⁻¹¹

At the RL a single jet is formed similar to a Taylor cone (Fig. 1 (l)), which may provide the path for single ions and macroions to be emitted⁶ (Fig. 1 (n)). An important result of our previous research is that a pronounced conical fluctuation precedes the transfer of the ions within the conical region⁶ (Fig. 1 (l)). Experiments have often observed two cones instead of one.^{44,45} We have found that rapid solvent evaporation may lead to supercharged droplets (above the RL) that may form two jets in diametrically opposite sites¹¹ as depicted in Fig. 1 (o). The multiple cones may enhance the probability of macroion ejection in these larger droplets.

In the nascent sprayed ensemble of droplets, the majority of the macroions will be found on the droplet surface, thus, they will be more susceptible to ejection either via jets or other droplet fluctuations appearing under highly non-equilibrium conditions that the droplets may be found. Thus, atomistic modeling of the minute nanoscopic droplets does not account for a number of possible macroion charging mechanisms as it is discussed in detail in the next section.

Here, we perform a systematic study to examine whether ejection of an unstructured linear macroion such as PEG and proteins is a dominant mechanism of release in droplets composed of a few thousands H_2O molecules and the possible charging mechanisms. We consistently find that ejection of a protonated peptide and protein is of low likelihood in droplets composed up to a 2.3×10^4 H_2O molecules (equimolar radius of 5.6 nm). By elimination, we suggest, that any possible ejection observed in experiments may come from capturing of a macroion into Rayleigh jets. We also identify three new factors that enter the charging of linear macroions that have not been recognized in earlier studies: (a) Effect of droplet curvature

in the conformation of a linear macroion; (b) Role of conical shape fluctuations in low probability events of macroion ejection; and (c) Partial extrusion of a macroion near the RL may be viewed as a Taylor cone.

A critical view of macroion release from droplets

An early review by Kebarle⁵¹ describes the initial efforts in the literature toward understanding the mechanisms of macroion charging and release from droplets. In Ref.⁵¹ two mechanisms of linear protein release are described. One of them was proposed by J. Fenn, who suggests that proteins or other analytes desorb from droplets by capturing an amount of charge that is covered by their area, which is in contact with the droplet surface.¹⁴ According to this conjecture, a protein exposes a charged portion on the surface, this part is extruded from the surface similar to the manner that a single ion escapes in the ion evaporation mechanism⁵²⁻⁵⁴ (IEM), and finally the extruded part pulls out the rest of the chain until the chain is desorbed.⁵⁵ Fenn was using the term “ion desorption mechanism” (IDM) for the ejection of macroions from droplets in analogy to IEM.^{14,33,56} Another mechanism was proposed by P. Kebarle, where a protein found on a droplet’s surface leaves via a significant oscillation of the droplet shape that expels a progeny droplet containing the protein.⁵¹ In both propositions, it is expected that the protein is found near the vapor-droplet interface. Considering that the ensemble of droplets has a high proportion of interface, the likelihood of a protein to be near the interface is substantial. The conducting nature of the droplet is another important force that drives a protein near the surface. It is noted that the Fenn and Kebarle propositions do not clearly define the droplet size from where the proteins are released. Nevertheless, Kebarle’s mechanism implies that the droplet has to be substantially larger than the protein in order to undergo such a large deformation. Fenn’s mechanism does not consider the role of the droplet’s shape fluctuations, such as the

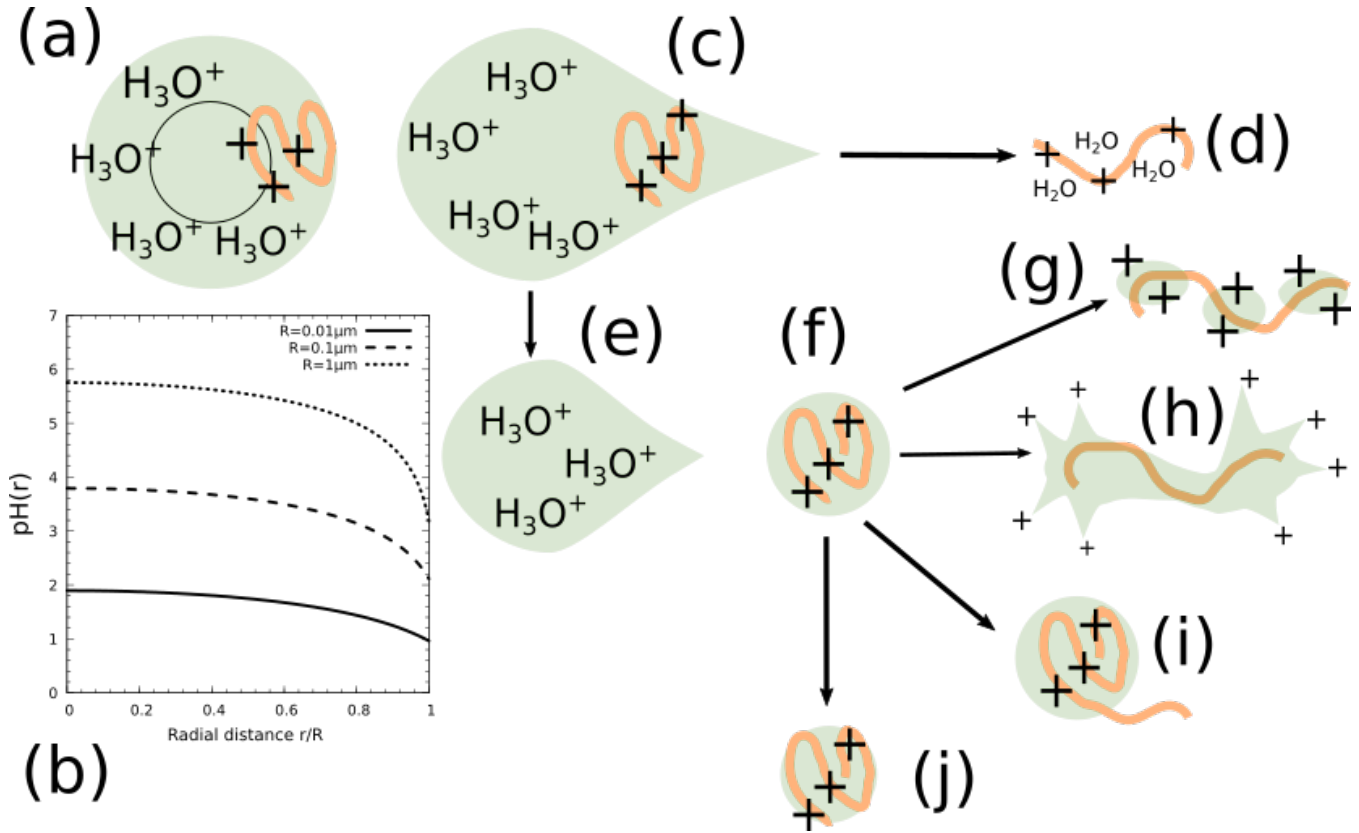


Figure 2: Schematic representation of the process of transfer of linear proteins from a charged droplet near the Rayleigh limit to the gaseous phase in an electrospray process. The color coding and the meaning of charge signs are the same as in Fig. 1. (a) Charged droplet near the Rayleigh limit. (b) pH profile as a function of the distance from a droplet's center of mass (COM) for droplets of various sizes from the solution of the Poisson-Boltzmann equation for a spherical geometry.^{46,47} In the x-axis r denotes the distance from the droplet's COM and R the droplet's radius. (c) Rayleigh jet formation on the droplet surface that may capture an entire chain or a segment of it. (d) A solvated chain may be entirely ejected from the jet or a segment may be ejected. (e) The jet may release a droplet containing the macroion. It is very likely that additional simple ions will not be released in the droplet containing the macroion. (f) The droplet may take "pearl-necklace" conformations.⁴⁸ (g) The droplet may become "star-shaped"⁴⁸. (h) The droplet may gradually release a linear macroion.^{34,48-50} (i) The droplet may shrink and a protein (compact or linear) may transfer protons to the surrounding H₂O molecules.⁴⁶ Details of all the steps are discussed in the text.

conical fluctuations we have identified and the the Rayleigh jets⁶ that they may play a role in a macroion’s charging and release. Both mechanisms are captured in continuum theory we have developed,^{1,35} since atomistic modeling is limited in minute nanodroplets. The charging of PEG is an excellent example that can be used to test Fenn’s proposition in minute nanodroplets. A systematic change of the macroion and droplet size may allow us to extrapolate the results in larger droplets.

In 2011, for the first time we presented direct evidence of the ejection³⁴ of linear macroions from droplets by using atomistic modeling of the sodiation (or lithiation) of poly(ethylene glycol) (PEG). We studied the sodiation of PEG within different solvents (H₂O, CH₃CN, CH₃OH) and in water with different ions (Na⁺, Li⁺, Ca²⁺). The PEG charging and extrusion mechanism have been tested with different force fields and simulation codes and the results show remarkable consistency.^{34,49,50,57,58}

The similarities between PEG and proteins have been addressed by de la Mora who notes¹⁵ “Proteins have been by far the species most studied by ESMS. However, most related data have involved denaturing conditions, with geometrical ambiguities similar to those with PEGs, both for the ion and for the drops producing them.” For proteins the direct protonation cannot be observed yet in atomistic modeling because of the complexity of the interactions that require quantum chemistry modeling, long time scale for conformational changes that may lead to a possible extrusion and strong dependence of the phenomena on force field parameters.⁵⁹

Konermann et al. using atomistic modeling reported that myoglobin in charge states +17 and +23 is fully ejected from droplets composed of $2.0 \times 10^4 - 2.3 \times 10^4$ H₂O molecules and they named it the chain-ejection mechanism^{60,61} (CEM). CEM hypothesizes the charging of the macroion in a manner identical to that of the PEG sodiation (or lithiation), but with an imaginary proton in the position of Na⁺. The proton does not have any atomistic presence in the modeling and does not transfer on the chain as Na⁺ or Li⁺ do in PEG. CEM

does not account for the fact that there are different chain extrusion mechanisms depending on the solvation energy of the chain.¹

Results from our previous research lead us to synthesize the picture shown in Fig. 2 about the charging and release of macroions from droplets larger than those that can be modeled atomistically. Figure 2 presents in more detail mechanisms of protein charging and release in the region shown in Fig. 1 (c)-(g).

There are two possible charging and release mechanisms of proteins (linear or compact) that cannot be captured by the atomistic modeling of the minute nanodroplets but have been inferred from continuum modeling³⁵ and by the atomistic modeling of the smallest jet.⁶

Charging of a linear protein with the assistance of the jet Differently from the conducting body of a charged droplet, a conical jet has electric field that attracts ions. It is likely that a segment of a linear protein near the surface is caught in the cone and the transfer of the H₃O⁺ ions in this region facilitate the charging of the protein. The cone may lead to a partial or complete extrusion of a linear protein.

Protonation of a protein in large droplets and emission from a jet Charging of a protein (linear or compact) can occur in the outer low pH layer of droplets with radius of at least a few tens of nanometers. We have shown (Fig. 2 (b)) that depending of the droplet radius, an outer layer of considerable thickness has significantly lower pH than the bulk of the droplet. The likelihood for a protein to be in this layer is high because of co-operating energetic and entropic factors. Once the protein is charged it is likely to be captured in a Rayleigh jet (Fig. 2 (c)-(d)). In previous research we have estimated a jet angle of 20° in an aqueous droplet. If the base of the jet is approximately the size of the protein, then we can estimate the radius $R_{emitted}$ of the emitted droplet containing the protein, which will be $R_{emitted} = R_P + 0.33R_P$, where R_P is the radius of the protein. Thus, a compact protein will be released surrounded by one or two layers of H₂O, while a linear protein will be sol-

vated with the corresponding amount of H₂O along its backbone. In larger droplets the base of the cone can be larger than the protein size, thus more H₂O layers can surround the protein. Once the droplet is emitted, if the protein unfolds then it may form pearl-necklace conformations (Fig. 2 (g)), star-shapes (Fig. 2 (h)) or it may show a gradual extrusion (Fig. 2 (i)) as we have discussed in previous work.⁵⁰ A mechanism where a protein in a small droplet can release charge has been discussed in previous work.⁴⁶

Regarding, the capture of the protein in a jet, one may argue that since there are at most two proteins (or protein complexes) in a droplet, the likelihood to be caught in a jet is low because (i) there are many more simple ions than a protein, and (ii) in general lack of correlation between the ion location and jet formation.^{6,11,54} However, the likelihood may increase because in slightly supercharged droplets multi-jets may appear^{6,11,54} and also, a loosely structured protein may occupy a significant area on a droplet’s surface that may increase the likelihood for a segment of it to be caught in a jet.

Temperature will play an important role in the charge state and release of proteins. The temperature of droplets has not been established yet^{24,25,62,63} partly because it will depend on the details of the instrument and the specific experiment. Factors that affect the temperature of microdroplets, whose temperature has been mostly studied,^{62,63} are evaporative cooling, conductive thermal transfer with the sheath gas, friction with the background gas. Temperature measurements that have been reported for microdroplets are in the range of 270 K to 307 K. For speeding up solvent evaporation atomistic modelling has been performed in very elevated temperature of 370 K or higher that may not be representative of experimental conditions. Methods of effective treatment of solvent evaporation at room temperature have been reported.⁶

The various scenarios of protein charging and release can lead to the charge state of proteins because in all the scenarios the proteins are found in a highly acidic environment.

Systems and Simulation Methods

Molecular dynamics (MD) simulations of aqueous charged droplets which also include poly(ethylene glycol) (PEG), protonated peptides, protonated myoglobin and Na⁺ ions were performed by using the software NAMD version 2.12.⁶⁴ For comparison with other works in the literature, simulations of myoglobin in certain charge states were also performed with GROMACS 2018.3.^{65–67} Details of the set-up are discussed in the next paragraphs for every macroion. Visualization of all the trajectories was performed by using VMD 1.9.2.⁶⁸

PEG and protonated peptides

In order to examine the likelihood of ejection of unstructured linear macroions, we selected poly(ethylene glycol) (PEG), and protonated peptides with a variable degree of hydrophobicity as representative examples. The systems and conditions are described in Table 1.

PEG was composed of 54 monomers (PEG54) and was embedded in droplets composed of 5×10^3 and 10×10^3 H₂O molecules. A number of Na⁺ ions were added so as the systems are near the RL. PEG54 is long enough to capture up to a maximum of 4Na⁺ ions.^{34,49} We selected a relatively short PEG for which is feasible to directly simulate its charging in aqueous droplets considerably larger than its size. This realistic system will allow us to infer charging mechanisms in droplets much larger than those that can be atomistically modeled so far. The structure of PEG54 and force field parameters were generated using CHARMM-GUI.^{69–71} The water molecules were modeled with the modified-TIP3P (mTIP3P) model.

We also prepared protonated peptides with hydrophobic segments composed of valine (Val) residues and a few single charged lysine (Lys⁺) residues in between these segments. Different arrangements of valine segments and Lys⁺ were tested. We performed equilibrium and non-equilibrium MD simulations on three model protonated peptide sequences (Val₆–Lys⁺)₃–Val₆, (Val₁₀–Lys⁺)₃

and Val₁₀-Lys⁺-Val₁₀ embedded in sodiated aqueous droplets. The prevalence of hydrophobic segments is intended to increase the peptide’s propensity for the droplet’s surface and thus, make it more prone to ejection. The protonated peptide was solvated in ≈ 2100 H₂O molecules, and 11 Na⁺ ions were added to bring the total charge of the system to 14 e for (Val₆-Lys⁺)₃-Val₆ and (Val₁₀-Lys⁺)₃-Val₁₀ and 12 e for Val₁₀-Lys⁺-Val₁₀ (Table 1). The protonated peptides were modeled with CHARMM forcefield. The water molecules were modeled with the modified-TIP3P (mTIP3P) model. The Rayleigh limit of the droplet were calculated with the surface tension of the water model used at the simulation temperature.^{72,73} At $T = 300$ K, the value of surface tension is taken to be 0.0523 N/m and at $T = 350$ K to be 0.0432 N/m.

Newton’s equations of motion were integrated using the velocity-Verlet algorithm with a time step of 1.0 fs. All long range forces were computed directly.

For the peptides, two types of simulations were performed with NAMD v.2.12: (a) Equilibrium simulations where the droplet was placed in a spherical cavity of radius 20.0 nm by using spherical boundary conditions. The cavity was sufficiently large to accommodate the shape fluctuations of the droplet. In the equilibrium simulations, the droplet reached vapor pressure equilibrium. (b) Non-equilibrium simulations where the droplet was placed in vacuo and was evaporated. We performed equilibrium simulations for each of the sequences at 300 K and 350 K, and non-equilibrium simulations at 350 K. The equilibrium runs were performed once at each temperature and the non-equilibrium runs in quintuples. For PEG54 only equilibrium simulations were performed in the same manner as the equilibrium simulations were performed for the protonated peptides. The number of water molecules ($N_{\text{H}_2\text{O}}$) reported in Table 1 is the initial number in the droplet. In the equilibrium runs ≈ 100 H₂O molecules evaporated and created an equilibrium vapor pressure within the cavity.

All the systems, with PEG and protonated peptides, were thermalized with the Langevin

thermostat with the damping coefficient set to 1 ps⁻¹.

Table 1: Systems and conditions of aqueous droplets with (a) PEG54 and Na⁺ ions, and (b) protonated peptides and Na⁺ ions. In the first column, the system composition is shown. The system composition is that for initializing equilibrium runs for the protonated peptides and PEG54 and for performing evaporation runs in vacuo (non-equilibrium setting) for the protonated peptides. The second column presents the initial number of H₂O molecules in the droplet ($N_{\text{H}_2\text{O}}$). The third column shows the temperature (T) of the systems.

Solutes	$N_{\text{H}_2\text{O}}$	T (K)
PEG54 + 29 Na ⁺	1×10^4	300
PEG54 + 25 Na ⁺	1×10^4	350
PEG54 + 18 Na ⁺	5×10^3	300
PEG54 + 18 Na ⁺	5×10^3	350
(Val ₆ -Lys ⁺) ₃ -Val ₆ + 11 Na ⁺	2183	350
(Val ₁₀ -Lys ⁺) ₃ -Val ₁₀ + 11 Na ⁺	2117	350
(Val ₁₀ -Lys ⁺ -Val ₁₀) + 11 Na ⁺	2080	350

Myoglobin

We performed non-equilibrium simulations of charged aqueous droplets containing a charged myoglobin dimer (either 1MBN or 1WLA) and Na⁺ ions. The charge state of the proteins, the temperature and the outcome of the simulations are shown in Table 2. 1MBN is the sperm whale myoglobin,⁷⁴ obtained by Watson in 1969. 1WLA is a wild-type recombinant horse heart myoglobin.⁷⁶ The sequence of aminoacids of the two myoglobin used in this study are similar, with 134 out of 153 identical amino acids. Both sequences were obtained with X-ray diffraction, but the resolution of 1MBN was 2.0 Å and 1WLA was 1.7 Å.

It is known that non-equilibrium simulations are very sensitive to the initial configuration of the system. Moreover, experimental techniques are not able to determine the exact conformation of the protein and its location within the

Table 2: Systems, conditions, and MD outcomes of protonated myoglobin⁷⁴ (1MBN and 1WLA) embedded in an aqueous droplet that also contains Na⁺ ions. The first column shows the type of myoglobin and its charge state used in the various MD runs. In the second column $N_{\text{H}_2\text{O}}$ has the same meaning as in Table 1. In the third column, total charge of the droplet is the sum of the charge state of myoglobin and the number of Na⁺ ions included in the droplet (details in the text). In the fourth column, the initial conformation of the protonated myoglobin to start the simulations is indicated. It is noted that the initial random coil conformation is generated from a zero charge bulk-phase equilibrium conformation for 1MBN, and from a gas-phase canonical charge conformation for 1WLA.⁷⁵ More details on the preparation of the initial conformation are found in the text. “Fully equilibrated” indicates that the charged protein is equilibrated within a droplet by restraining its position in the COM of the droplet or near its surface. In the sixth column, the outcome of MD simulations on protonated myoglobin’s location is summarized. Length of simulation is indicated in Fig. 7. In the seventh column the temperature, T , of the systems is presented.

Type & charge state	$N_{\text{H}_2\text{O}}$	Total droplet charge	Initial myoglobin conformation	Initial location of charged myoglobin	MD outcome of myoglobin’s location	T (K)
1MBN ¹⁷⁺	20058	+36	Random Coil	Center	Off-center	350
1MBN ²³⁺	22494	+36	Random Coil	Near surface	Near surface	350
1MBN ¹⁷⁺	22505	+40	Fully equilibrated	Near surface	Near surface	350
1WLA ²²⁺ [A]	22766	+47	Random Coil	Center	Partially extruded & rest dried-out	370
1WLA ²²⁺ [A]	23179	+47	Random Coil	Near surface	Partially extruded & rest dried-out	370
1WLA ²²⁺ [C]	22401	+47	Fully extended	Center	two sub-droplets at protein’s termini	350

droplet when the ESI sprayed droplet is at the nanometer scale. Therefore, we elected to start from multiple combinations of initial configurations where the protein is found in a coiled state and an extended state. In addition, we performed simulations where the protein is initially located in the center and near the droplet-vacuo interface.

1MBN Simulations of 1MBN¹⁷⁺ and 1MBN²³⁺ were performed using NAMD version 2.12. The charge pattern of the 1MBN¹⁷⁺ is as follows: All His residues are protonated (charge +1), all Asp and Glu residues are unprotonated (charge -1) except Asp27, Glu109 and Glu136 which are protonated (charge 0). The charge pattern of the 1MBN²³⁺ is as follows: All His residues are protonated (charge +1), all Asp and Glu residues are protonated

(charge 0).

The protein was modeled with the CHARMM36m force field⁷⁷ and the water was modeled with the mTIP3P model. The protein was solvated with $2.0 \times 10^4 - 2.25 \times 10^4$ H₂O molecules and the charge of the system was increased to +36 by adding Na⁺ ions (13 Na⁺ ions in 1MBN²³⁺ and 19 Na⁺ ions in 1MBN¹⁷⁺) (Table 2). The initial configuration for 1MBN were generated by stretching the protein in gas phase, then setting the charge of every atom to zero and let the chain relax into a loosely coiled conformation. This yields an initial conformation that lacks a well-defined secondary structure. These coiled conformations were then solvated and charged. We used the gaseous phase conformation in order to compare with the simulations in Ref.⁷⁵ In the Results and Discussion section we comment on the disadvantages of using a

gaseous phase conformation within the droplet.

Additional simulations were performed where the COM of 1MBN¹⁷⁺ and 1MBN²³⁺ were restrained near the droplet surface (Table 2) for relaxing the protein conformation before the cavity was removed and evaporation in vacuo (without the presence of the spherical cavity) was initiated. The relaxation of the conformation lasted for 5 ns. The change in the radius of gyration and the root-mean-square relaxation as a function of time are shown in Fig. S1 in SI.

1WLA For comparison, we used the charge patterns of 1WLA^{22+[A]} and 1WLA^{22+[C]} in Ref.⁷⁵ The exact charge pattern can be found in the Supporting Information of Ref.⁷⁵ https://pubs.acs.org/doi/suppl/10.1021/acs.analchem.8b02926/suppl_file/ac8b02926_si_001.pdf. The charge assignment of each residue and the simulation method is identical to that in Ref.⁷⁵

The protein was modeled with the CHARMM36 force field and the water was modeled with the TIP4P/2005 model.⁷⁸ The protein was solvated with ≈ 22500 water molecules and the charge of the system was increased to +47 by adding Na⁺ ions (Table 2). The Nosè-Hoover thermostat was used to thermalize the system at 370 K. The droplet was placed in a cubic simulation box with sides of 999 nm. The cutoff distance were set to 333 nm and long range electrostatic forces were evaluate directly. Water and Na⁺ ions that traveled further than 100 nm from the COM of the system was removed every 250 ps. The trajectory stitching method was used to continue the simulation once the H₂O molecules were removed. The length of the simulation was 40 ns.

The initial configuration for the 1WLA²²⁺ system were generated by relaxing the protein in gas phase for 100 ns. Specifically, it is written in Ref.⁷⁵ “Unfolded protein structures were initially produced by heating aMb (1WLA without heme) from 320 to 450 K in vacuum using canonical charge states over 20 ns. Conformers generated toward the end of these runs served as starting points for droplet simulations.” In Ref.⁷⁵ no information was provided of how the initial conformation was prepared. By exper-

imentation we found that 1WLA^{22+[A]}, [C] in the gaseous phase (bare of water) were extended when no cut-off was used in the electrostatic interactions, and it remained a loose coil when cut-off was used. Test simulations were performed with 1WLA^{22+[C]} in the extended form with no cut-offs. A fully extended conformation was obtained by simulating it in gas phase for 100 ns. The fully extended conformation was then solvated with layers of H₂O molecules to form a cylindrically shaped droplet. As the system relaxes, the droplet divided into two sub-droplets, each solvating the ends of the protein. We think that the origin of this separation is due to the interplay of two competing factors: minimization of the surface area of a water droplet, and maximization of the protein solvation. In order to have a compact droplet, the coiled conformation was used as an initial conformation.

It is emphasized here, that in the simulations of 1MBN¹⁷⁺ the manner in which the initial coil conformation was prepared was different from that followed for 1WLA^{22+[A]} and [C].

Drawbacks in simulations of proteins in droplets Here we note the uncertainties in the modeling of 1WLA^{22+[A]} and [C] as presented in Ref.⁷⁵ TIP4P/2005 reproduces the surface tension^{72,73} of water over a range of temperature, however, the CHARMM force field for proteins is parametrized with respect to a modified version of TIP3P (mTIP3P). A charged protein in general might be in a different conformation when used with water models that it has not been parametrized for it. In our opinion, it is more important to model well the interaction between the water molecules and the protein side chains than the surface tension of the droplet. Although mTIP3P reproduces lower surface tension of water than TIP4P/2005, the surface tension is a parameter in the fissility parameter (Eq. 1) that will determine the amount of charge that the system can hold for the particular surface tension. Therefore, using a water model that replicates the surface tension of water may not be necessary.

The trajectory stitching method utilizes a pseudo-PBC approach, where the droplet is

placed in a very large simulation box and where long range electrostatic interactions are calculated directly as opposed to using conventional Ewald sum methods. The evaporated water molecules are removed periodically and the velocity of each molecule is reassigned according to the Boltzmann distribution after evaporated water have been removed. However, under non-equilibrium conditions where rapid solvent evaporation takes place, the Boltzmann distribution may not be followed. Moreover, the simulations have been performed in very elevated temperature (370 K) that may not be relevant to experimental conditions.^{62,63} Methods for evaporating H₂O molecules without relying on the trajectory stitching method and for efficient evaporation of the solvent molecules even at room temperature have been proposed.⁶ The selection of the initial conformation of the protein from the gaseous state is another factor that biases the outcome of the MD trajectories. The effect of this bias is discussed in the Results and Discussion.

Results and Discussion

Charging of PEG provides insight beyond minute nanodroplets

PEG may be considered to share some commonalities with intrinsically disordered proteins (IDPs) because of their flexibility in their backbone. PEG has the great advantage that it allows one to directly observe the transfer of ions from H₂O to the chain and its extrusion from a charged droplet.³⁴ Even though we have studied the PEG charging mechanism^{34,49,50,57,58,79} a remaining question is whether our observations in small nanoscopic systems are transferable to larger droplet sizes and longer macromolecules than those atomistically modeled. To mimic these large droplets, we scale down the problem to a large droplet size relative to the length of PEG. Specifically, we model PEG54 in droplets comprised 10×10^3 H₂O molecules and 5×10^3 H₂O molecules and Na⁺ ions at $T = 300$ K and 350 K (Table 1). During the entire trajectory within the spherical cavity a

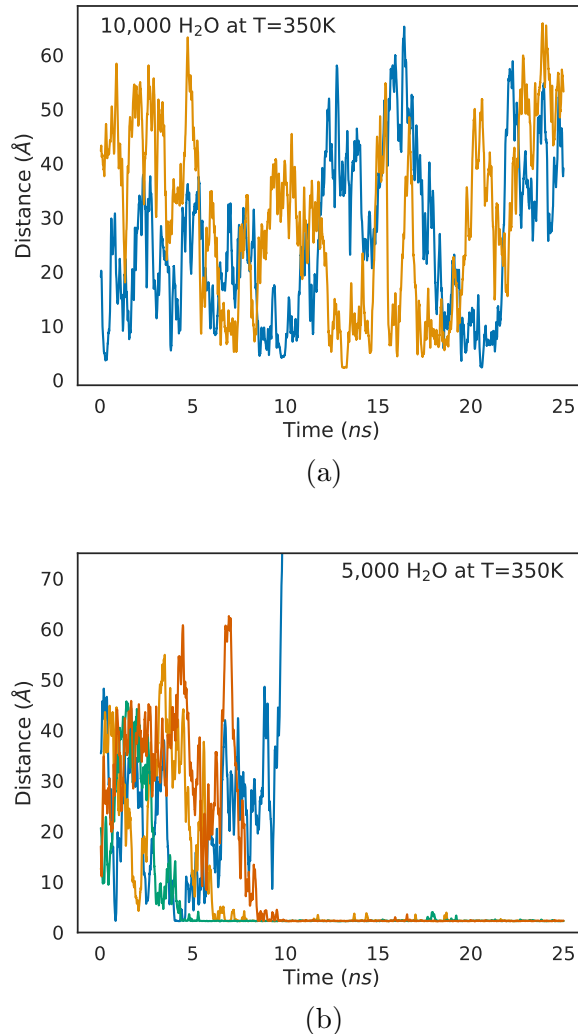


Figure 3: Typical sodiation events of PEG in aqueous droplets as a function of time. (a) 10×10^3 H₂O molecules, 25 Na⁺ ions and PEG54 and (b) 5×10^3 H₂O molecules, 18 Na⁺ ions and PEG54, at 350 K (see Table 1). The y-axis measures the least distance of a particular Na⁺ ion from any PEG54 oxygen atom. Several transient sodiation events were observed in the course of the simulations, but for clarity, only the PEG54 binding to two and four Na⁺ ions in systems (a) and (b), respectively, is shown. Similar graphs but at 300 K are shown in Fig. S2 in SI.

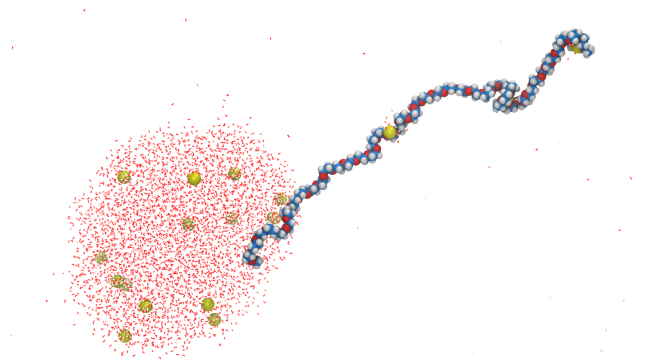
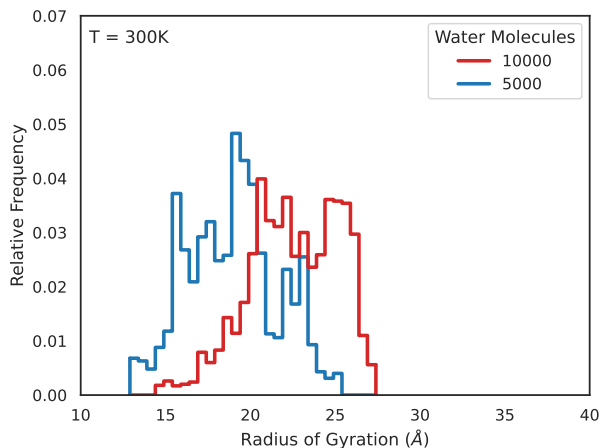


Figure 4: Typical snapshot of PEG54 at 350 K in a droplet comprised 5×10^3 H_2O molecules (O colored in red and H in white) and 18 Na^+ (colored in yellow) ions (see Table 1). PEG54 captures three Na^+ ions and escapes. The sizes of PEG and Na^+ ions have been enlarged relative to H_2O molecules for visualization purposes.

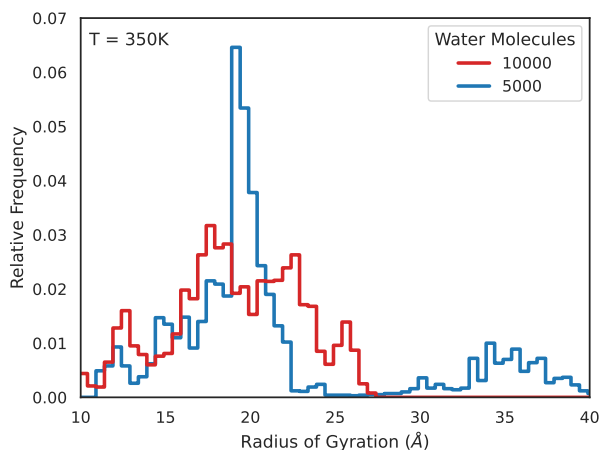
few Na^+ ions escape from the parent droplet. The droplet composed initially of 5×10^3 H_2O molecules emits one Na^+ and that of 10×10^3 H_2O molecules emits three Na^+ ions. Decisive factors in the charging and release of PEG and by extension in any linear macromolecule are: the ratio of the charge on the macroion while still attached in the droplet's body to the free charge in the droplet,^{34,49,57,58} the temperature of the system, and the presence of counterions.⁷⁹ Here we identify a new factor, which is the effect of the droplet curvature on the PEG conformation and thus, on the charge state.

Figure 3 (a) and (b) show the extent of time that Na^+ ions bind to the PEG backbone. In droplets comprised 10×10^3 H_2O molecules at both 300 K and 350 K, Na^+ ions transiently bind to PEG. Differently, in a smaller droplet, of 5×10^3 H_2O molecules Na^+ ions bind long enough (permanent sodiation) for the sodiated PEG to extrude from the droplet as shown in Fig. 4. In both droplet sizes, Na^+ are present for binding. The difficulty of a long-living sodiation in a larger droplet comes from the PEG conformation.

Figure 5 (a) and (b) show the histograms of PEG54 radius of gyration (RG) for two droplet sizes. In both temperatures the conformation of PEG in the 10×10^3 H_2O -molecule droplet is more extended than in the 5×10^3 H_2O -



(a)



(b)

Figure 5: Distribution of radius of gyration of PEG54 at (a) $T = 300$ K and (b) $T = 350$ K in droplets comprised 5×10^3 H_2O molecules and 18 Na^+ ions, and 10×10^3 H_2O molecules and 25-29 Na^+ ions (Table 1) The time evolution of RG is shown in Fig. S3 in SI.

molecule droplet. In the 5×10^3 H₂O-molecule droplet, at $T = 350$ K (Fig. 5 (b)) there is a second broad peak between 30 Å-40 Å, which is due to the extruded linear sodiated PEG54. The more extended PEG54 conformation in the larger droplet is caused by the droplet curvature. Thus, even though Na⁺ are available for binding, the droplet curvature prevents the coiling of the chain that may lead to a long-living sodiation.

Here we synthesize the overall picture that we have obtained by systematic simulations of charging of PEG with Na⁺ (also Li⁺ and Ca²⁺ ions) in previous research^{34,49,50,57,58} and in the present studies in aqueous nanodroplets composed up to ten thousand H₂O molecules (equimolar radius 4.2 nm). The new results allow us to understand the mechanism in droplet sizes that are not accessible to atomistic modeling yet.

The general mechanism we have identified for the charging of PEG regardless of its length and the droplet’s size is as follows: Evidence from previous simulations^{34,49,50} has shown that a PEG of specific length can be charged in droplets of various sizes and partially extrude. Specifically, in previous research⁵⁰ we found that PEG64 can be charged via long-living (we call it permanent) sodiation in droplets with ≈ 7000 , 3500 and 2000 H₂O molecules. Previous results are complemented by the present study that shows for the first time, that for a PEG of specific length there is a *critical* droplet size beyond which, PEG is charged intermittently. The life-time of the sodiation events is shorter than the time required for the PEG backbone to unzip from the droplet surface and release by carrying the ion with it.

We have found that the first permanent sodiation takes place on the droplet surface in 10%-15% overall charge below the RL in droplets of different sizes.^{34,49,50} If we compare this value with the X (defined in Eq. 1) values that a Rayleigh jet is formed,⁶ we conclude that it is the range of 10% - 15% charge below the RL where the fluctuations will be intensified and the critical point of the Rayleigh instability is approached. Thus, the first transfer of an ion to PEG occurs at the onset of the intense shape

fluctuations near the RL. The captured Na⁺ ions may be escaping ions from the water body due to intended formation of a jet. Since PEG may capture the ions, the formation of the jet may be avoided in certain cases. We expect that an entire PEG or a segment of it can be also captured by a Rayleigh jet when formed. For droplets with fewer than ≈ 1000 H₂O there are some more details that enter the charging mechanism because of their large relative shape fluctuations that bring the value of X much less than 1 for droplet stability.⁹

Once an ion is “permanently” captured by PEG, a part of the PEG chain extrudes. We have found that in the majority of the PEG simulations at 300 K and 350 K the chain partially extrudes and then a part of it dries-out. Drying-out has been observed significantly more frequently than ejection for the following reason: There are many more free charges (Na⁺, H₃O⁺) in a droplet than macroions. The likelihood of the single ion release is much higher than of the macroion’s. Since single solvated ions are released, and also the chain immersed in the droplet may be charged, the droplet may not have a critical charge to repel a segment of the chain.

Now, we ask the question: In which droplet size does PEG sodiation occur? The present in combination with previous studies^{34,49,50,57,58,79} show that charging of PEG is highly likely to occur in droplets much larger than the ones that can be atomistically simulated. The longer the PEG, the larger the droplets in which it can be charged. There is a *critical* droplet size above which short-lived charging of PEG may occur. Lower charge density in larger droplets may be an additional factor that prevents the ejection of a macroion from the droplet.

Similar mechanisms need to be considered for the charging of proteins. Unfortunately, the proteins are very restrictive to a systematic study of their charging and possible extrusion mechanism from droplets. Moreover, the outcomes of simulations may be strongly biased by the selection of the protein’s initial conformation. A similar bias does not hold for at least the shorter chains of PEG.

If we were to transfer the transient sodiation

to the protonation of a protein we may infer that changes in the solvation of a protein due to droplet size and the time required for conformational changes will affect a protein’s ability to capture a proton. Thus, high proton availability and an extended protein conformation does not necessarily lead to a higher protein charge state relative to a less extended conformation, if considerable conformational changes are required for the extended conformation to host the proton.

Release of protonated Valine-Lysine peptides from nanodroplets - A rare event

Droplets comprised ≈ 2100 H_2O molecules, a peptide comprised Lys+ and Val residues (Table 1) and Na^+ ions were simulated under equilibrium conditions (where an equilibrium is established between the droplet and its vapor within a spherical cavity) and non-equilibrium evaporation runs in vacuo. The RL for these droplets at their initial size is +13 if we consider that the peptide is equivalent to 215 H_2O molecules. Droplets that initially have charge +14, release one or two Na^+ ions. Direct visualization of the systems shows that the Val residues lie on the surface of the droplet, and the side chains of the protonated lysine residue point toward the interior.

It is noted that, in a nanometer scale droplet, hydrophobic and hydrophilic residues behave opposite to that of bulk solution. In a bulk solution, the hydrophobic residues prefer to aggregate and form a hydrophobic core, buried in the interior of a protein while the charged (hydrophilic) residues lie on the exterior of the protein. When a quasi-linear and flexible protein is located near the surface of a nanoscale droplet, the hydrophobic core may unfold and lie on the surface of the droplet, solvated by minimal amount of water in order to lower the solvation energy penalty. The hydrophilic residue, in general prefer to be well solvated, therefore when they are forced to the surface, the side group will tend to point inwards, which enable solvation stabilization. This is also supported by

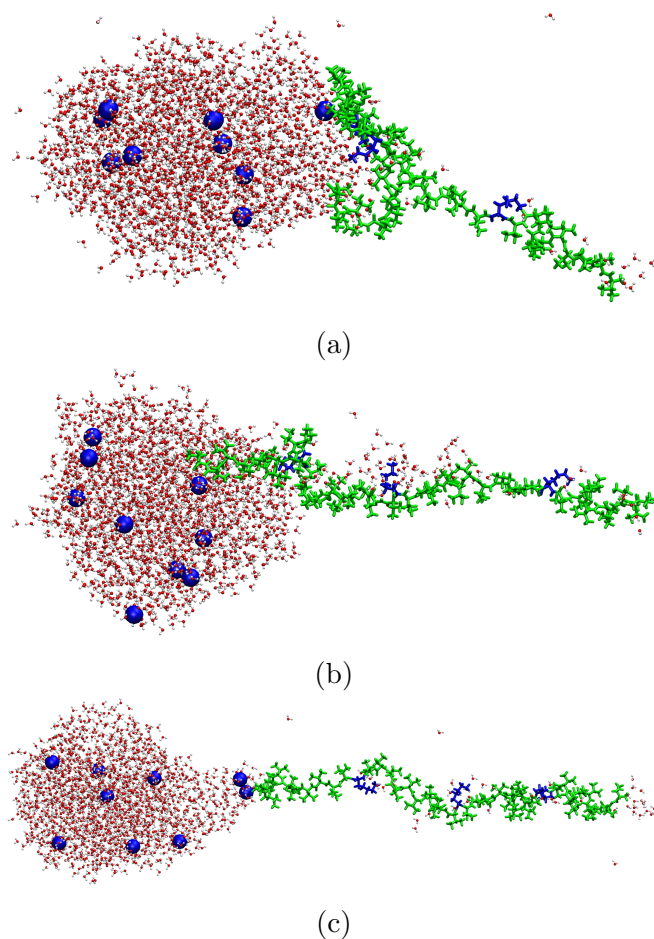


Figure 6: Typical snapshots of the *rare* event of $[(\text{Val}_{10}-\text{Lys}^+)_{3}-\text{Val}_{10}]$ ejection from an aqueous droplet. The lysine and valine residues are shown along the chain by the blue and green colour residues, respectively, and the Na^+ ions are represented by blue spheres. The O sites of the H_2O are shown by red spheres and the H sites by white. (a) First step of the extrusion of a solvated protonated peptide from a droplet composed of ≈ 1925 H_2O molecules. We consider this configuration as the time origin. (b) Further extrusion of the chain from a droplet composed of ≈ 1735 H_2O molecules at 4.4 ns from the time 0. (c) Complete ejection of the chain from a droplet composed of ≈ 1694 H_2O molecules at 5.2 ns from time 0. The ejection is assisted by two Na^+ ions at its attachment point to the droplet. Additional snapshots are shown in Fig. S3 in SI.

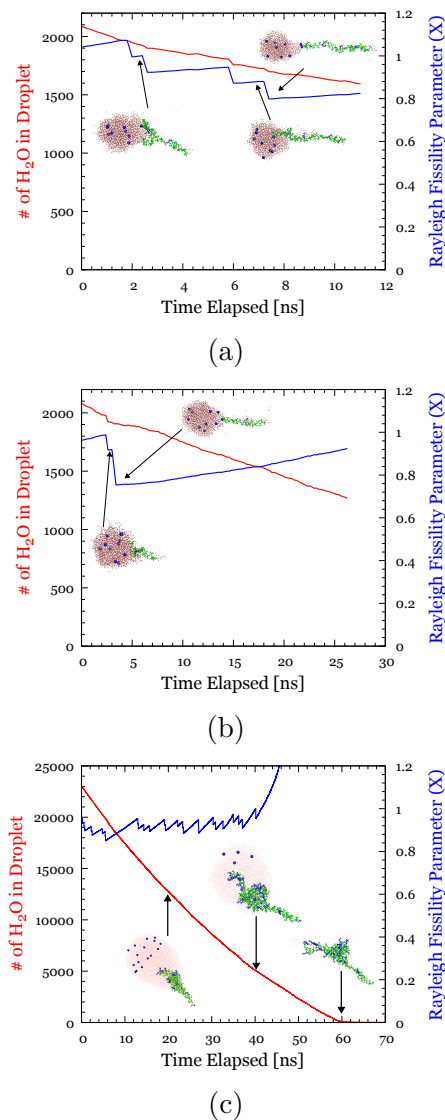


Figure 7: Time evolution of number of H₂O attached to the droplet and Rayleigh fissility parameter, X defined in Eq. 1 in a drying-out process. (a) (Val₁₀Lys⁺)₃Val₁₀. (b) Val₁₀Lys⁺Val₁₀. (c) 1WLA²²⁺. X is calculated by assuming a spherical shape of the droplet. It is noted that in (c) $X > 1$ beyond 40 ns because the protein dries-out. In the estimation of X only the charges within the droplet are included.

experimental data in electron cryo-microscopy where it has been shown that proteins tend to adsorb to the air-water interface with a preferred orientation, or that they may even become partially or fully unfolded at the interface.⁸⁰

Equilibrium simulations (where vapor and droplet are at equilibrium within a spherical cavity) are used to establish a reference point for comparisons of the peptide's conformations. Initially, in the evaporation simulations (non-equilibrium) in vacuo where the peptide does not extrude, the protonated peptides have the same conformation as in the equilibrium simulations. Moreover, no extrusion was found in the equilibrium runs.

In the non-equilibrium simulations it is found that in all cases the extrusion of the chain occur less frequently than the drying out. For (Val₆-Lys⁺)₃-Val₆, in all five evaporation simulations performed, protonated peptide extrusion was not observed, instead the droplet dries out. During the course of the simulation, Na⁺ can be seen ejecting from the droplet, which indicates, that the ions are much more mobile than a chain-like macromolecule.

We increased the number of valine residues in between lysine residues, to investigate whether the valine residue compact similar to what we observed with pure poly-valine - and whether a hydrophobic core might form in this case. For [(Val₁₀-Lys⁺)₃-Val₁₀] three out of the five runs did not show any extrusion, one run showed partial extrusion and one run ejection of the protonated peptide. Typical snapshots from the ejection process are shown in Fig. 6. It is noted that the ejection was assisted by the presence of two Na⁺ in a conical fluctuation at the end of the chain found in contact with the droplet (Fig. 6 (c)).

For [Val₁₀-Lys⁺-Val₁₀] extrusion was observed only in one case out of five runs. Similarly to [(Val₁₀-Lys⁺)₃-Val₁₀], the extrusion was also assisted by the Na⁺ ions accumulated in a conical shape fluctuation. Typical snapshots of this system are shown in Fig. S5 in SI.

Figure 7 (a) and (b) show the reduction of the H₂O molecules and the variations in the value of X (see Eq. 1) for (Val₁₀Lys⁺)₃Val₁₀

and Val₁₀Lys⁺Val₁₀, respectively, as a function of time in a drying-out process. Large decrease in the value of X is associated with the release of a macroion segment as shown in the snapshots included in the figure.

From all the simulations that were performed, even with highly hydrophobic peptides, it is found that the partial extrusion is of low frequency and the ejection of a protonated peptide is even more rare. This is due to the fact that the Na⁺ ions may be released faster than the chain, and that even the hydrophobic residues form H-B with the droplet.⁵⁸ The interplay between solvation of the chain and repulsion from the charges of the same sign in the droplet has been discussed in detail in previous articles.^{1,35} It is noted here that the charges of the same sign within the droplet can be the part of the solvated chain itself that may be charged. Thus, the presence of free ions is not the only source for repulsion, and in fact, the free ions are not necessary for triggering a chain extrusion.

In previous work^{6,11} we demonstrated the significance of the conical fluctuations on the droplet surface in the release of simple ions and in the formulation of the ion evaporation mechanism.^{52,53} It appears that a rare event, where a conical fluctuation captures a protein’s charged site or it allows for other ions (e.g. H₃O⁺ or Na⁺) to assist in the repulsion of the chain, may lead to partial chain extrusion or detachment from the droplet.

For the conical fluctuations to play a role in the extrusion of the chain, the droplet should be near the RL. The fact that an extrusion may take place near the RL is along J. Fenn’s conjecture that the charge density should be appropriate for macroion desorption.^{14,33} However, Fenn’s conjecture did not consider the critical role of the conical fluctuations in the ejection mechanisms. For PEG a very similar mechanism of extrusion has been found.^{34,49}

Charged myoglobin in aqueous droplets - A Taylor cone formation

1MBN²³⁺ A semi-compact configuration of 1MBN²³⁺ was generated by removing all partial charges on the protein, and letting it equilibrate for 1 ns. We then solvated the protein in a droplet of ~ 22500 H₂O molecules, restored its charge, and added 13 Na⁺ to bring the droplet’s overall charge slightly below the RL (Table 2). The RL for this droplet size corresponds to charge +43.8. The protein was placed both in the center of the droplet and near the surface. We have only observed evaporation of water, ejection of simple ions and protein undergoing conformational changes. In both runs, the protein was well solvated with water even after 25 ns, thus no partial extrusion of the protein was observed.

Coiled 1WLA²²⁺ A coiled 1WLA equilibrated in the gaseous phase was placed in the droplet’s center and its charge was restored to +22 (details are described in the “Systems and Simulation Methods” Section). It was observed that almost all Na⁺ ions diffused near the surface in 1 ns while the protein diffused much slower toward the surface. The protein is expected to migrate near the surface because of the conducting nature of the droplet. The diffusion time of 1WLA²²⁺ from the center to the surface was at least twice as long as those reported in Ref.⁷⁵ This difference may not be critical for the protein extrusion. The droplet shape underwent a significant fluctuation when the droplet moved near the surface. Snapshots of the entire process up to the protein’s drying is shown in Fig. S6-S8 in SI. It appears that the migration of the protein to the surface is enhanced by the oblate-prolate breathing motion of the droplet. However, these large fluctuations may occur because the protein is already charged. The motion of the ions becomes correlated because there is not enough water for screening the ions in this high charge density system. It is observed that the relatively hydrophobic part of the protein extruded first, while the hydrophilic and charged part of

the protein stayed in the droplet interior and dried-out as shown in Fig. 7 (c). A close-up of the extruded hydrophobic portion is shown in Fig. 8. At the onset of the extrusion, the droplet stretches into an oval shape. As the protein is partially released from the droplet, the droplet relaxes back into a spherical shape (Fig.S6 in SI). The protein did not completely eject but it dried out (Fig. S7-S8 in SI).

The same simulation outcome was observed with a different initial condition where a coiled 1WLA²²⁺ conformation was placed on the droplet surface, within the electric double layer of the droplet. The possible outcomes of this initial condition are (a) protein diffusion towards the interior and (b) protein extrusion from the droplet. Since the protein starts from a conformation that has been relaxed for the gaseous state it is bound to extrude. From both initial conditions, only a portion of the protein was extruded, while the rest of the protein dried-out of solvent.

For a highly charged protein such as the ones used here, a partial extrusion from small nanodroplets may be viewed as the formation of a *Taylor cone*. In previous research we have demonstrated the significance of the conical fluctuations on the droplet surface for the release of ions.^{6,11,54} We also note that in all the simulations of the peptides and myoglobin the charge is already present in their backbone. If initially the protein had a low charge then it would have a more organized structure. Since the outer surface layers of a droplet holds higher simple ion (e.g. (H_3O^+) concentration than the bulk interior,⁴⁶ the protein is subject to a lower pH (see Fig. 2(b)). The charging on the surface, may lead to its conformational changes. These conformational changes may require much longer time than the simulation time. Performing the simulations using gas phase equilibrated protein structures *biases the simulation outcome* since the natural states are delivered from the bulk solution.

It is emphasized here that these simulations are under non-equilibrium conditions. Consequently, the collection of sufficient statistics for such large systems is a formidable task. The simulations presented here along with those re-

ported by Konermann et al. on myoglobin complete ejection⁷⁵ demonstrate the variability of the results depending on the initially selected protein conformation and its location in the droplet. A highly charged chain equilibrated for the gaseous state, is bound to extrude or possibly to be completely ejected because the conformation is prepared to provide this outcome. Moreover, every highly charged protein placed near the surface will extrude because of Coulomb repulsion within the chain.

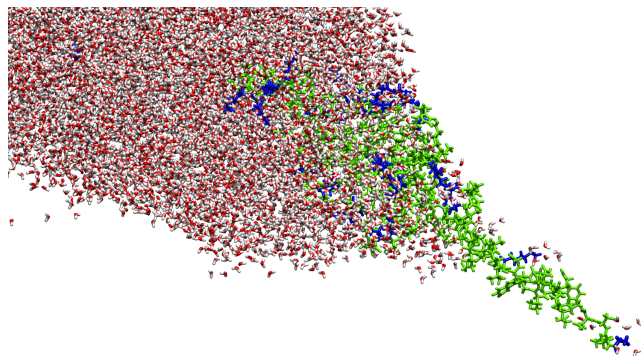


Figure 8: Magnification of a segment of a droplet to show the partial extrusion of 1WLA²²⁺[A] from an aqueous droplet (see Table 2). The charged residues are colored in blue and the uncharged residues are colored in green. Na⁺ ions are depicted by blue spheres. The color coding of the H₂O molecules is the same as in Fig. 4.

Conclusion

We used molecular dynamics to address two questions: (a) The likelihood of extrusion of poly(ethylene glycol) (PEG), linear protonated peptides and protonated myoglobin from an aqueous charged droplet. (b) Obtain insight on how macroion charging takes place in droplets larger than those that can be modeled at the atomistic level. PEG (and like macromolecules) is the only molecule for which we can directly observe its charging by metal ions and its release from a charged aqueous droplet.

We have found that PEG molecules with length between 54 to ≈ 100 monomers in droplets composed up to several thousands of H₂O molecules, become sodiated and extrude

from the droplet. The longer chains extrude partially, while the shortest ones (with 54 and 67 monomers), depending on the temperature, may be completely released.^{34,50,57} However, the atomistic modeling is limited to a narrow window of droplet sizes in the latest stages of a droplet’s lifetime. In order to examine whether PEG can be charged in droplets larger than those that can be modeled atomistically we scaled down the problem to a large droplet size relative to the length of PEG. The charge state of the droplet was near the Rayleigh limit. We found that PEG54 in a droplet composed of $10^4\text{H}_2\text{O}$ molecules (equimolar radius of the droplet 4.2 nm) and Na^+ ions is frequently sodiated in a transient manner in contrast to smaller droplets where long-living (permanent) sodiation takes place. The permanent sodiation may lead to the detachment of sodiated PEG from the body of the droplet. Finding the existence of a critical droplet size that affects the PEG conformation and its charging and by extension that of other macorion, is significant, as it contradicts the intuitive belief that the more extended the macroion is on a droplet surface, the higher its charge state would be.

To summarize, there are several factors that affect the charge state of PEG, and by extension that of other macromolecules such as proteins. Firstly, the droplet’s shape fluctuations. The initiation of the charging of PEG and the extrusion of the first segment takes place 10%-15% below the droplet’s Rayleigh limit. At this degree of deviation from the Rayleigh limit the droplet’s shape fluctuations are the largest due to charge and the release of the ions is facilitated. Secondly, the temperature. Finally, a new factor was identified in this study, the droplet’s curvature. The example of PEG54 in a droplet of $10^4\text{H}_2\text{O}$ molecules shows that even though Na^+ ions are available to be captured by PEG, the stretching of the chain on the surface due to the droplet’s curvature prevents the folding of PEG around the ions. The relative size of length of PEG and droplet curvature is a factor that determines when long-living chain charging is feasible. Longer chains will be charged and possibly extrude in larger droplets that those that can be atomistically modeled.

Fenn’s ion desorption model (IDM) for linear macroion charging assumes that the free charges are distributed on the droplet surface at equal distance in order to minimize the electrostatic repulsion. Fenn suggested that the spacing of charges will decrease as a droplet shrinks, thus the analyte will be able to capture more charge. The availability of free ions in relation to the coverage of the droplet surface by a macroion is definitely a factor that determines the charge state of a macroion. However, one has to consider a dynamic location of ions in a thick outer layer⁹ of a droplet (that includes the electric double layer) than a static one. The present study complements Fenn’s intuitive mechanism by showing that it is not only the free ion availability but also the droplet’s curvature that affects the conformation of the macroion, and consequently its charging. Thus, a more stretched macroion on a droplet’s surface (that maximizes the coverage of the surface and thus, is more accessible to the ions) does not necessarily mean a higher charge state of the macroion or more facile charging.

Since protonation reactions cannot be explicitly modeled for proteins in these systems, the charging of PEG may offer possible scenarios that protons may be transferred to proteins. The CEM maps the mechanism of charging of PEG to unstructured proteins by replacing Na^+ with a hypothetical proton. However, for proteins it is still unknown at what droplet size the charging may take place and whether transient protonation plays a role. We suggest that it is possible charging to take place in the low pH region near the surface at larger droplets than those that we can model atomistically.⁴⁶

The peptides and myoglobin studied here were already carrying charge when simulated. This study revealed that: (a) Conformations of proteins taken from the gaseous state as it is often done in simulations of droplets, bias the simulation outcomes. (b) In the very small nanodroplets, possible ejection of proteins appears with low probability. (c) Partial extrusion of a protein, when it occurs, may be viewed as a Taylor cone.

In previous work we demonstrated the significance of the conical fluctuations on the droplet

surface in the IEM mechanism.^{54,79} Similarly, simulations indicate that a rare combination of events involving a conical shape deformation may play a role in a protonated peptide’s extrusion. It is emphasized that at the Rayleigh limit the conical deformation appears first and then charged species may enter the cone. The role of a conical deformation may be that (a) it captures a protein’s segment and assist its extrusion from the droplet surface; (b) it allows for simple co-ions (e.g. H_3O^+ or Na^+) in the vicinity of a protonated peptide to enter the cone and repel portion of the chain. This step may assist the chain to detach from a droplet. Possibly, the conical deformations may also assist in the charging of macroions. Understanding the chemistry in conical shapes is still an open question. The role of the conical fluctuations is robust because we have consistently observed them to play a critical role in IEM and here, in different systems containing the protonated peptide.

Atomistic modeling of droplets with macroions has taken place in minute nanodroplets, in the regime where a train of single ions cannot be released via Rayleigh jets. By simulating this narrow size regime, all the possible pathways of macroion release such as capturing of macroions in jets cannot be revealed. Thus, a question arises whether a possible protein extrusion mechanism found at the end of a droplet’s lifetime is part of the natural path of a droplet’s evolution. It is also noted that detection by simulations of a possible protein extrusion or ejection will be very sensitive to force field parameters.⁵⁹

Supplementary Material

(S1) Relaxation of 1MBN^{17+} in an aqueous droplet; (S2) Additional data for the charging and conformations of PEG; (S3) Typical snapshots of the rare event of valine-lysine protonated peptides extrusion from charged aqueous droplets. (S4) Typical snapshots of $1\text{WLA}^{22+}[\text{A}]$ partial extrusion and drying-out in an aqueous droplet. In addition a movie is provided that shows the transient charging

and extrusion of PEG54 in a droplet of 10^4 and 5×10^3 H_2O molecules, respectively.

Acknowledgments

S.C. is grateful to Prof. D. Frenkel, Yusuf Hamied Department of Chemistry, University of Cambridge, UK and Dr. Anatoly Malevanets for insightful discussions on the stability of charged systems. S.C thanks Prof. Dr. T. Leisner and Dr. T. Dresch, Karlsruhe Institute of Technology, Germany, for discussions on the jets and droplet acidity. VK and SC acknowledge discussions with Dr. Myong In Oh (SC group) and Dr. Mahmoud Sharawy (SC group), who were former graduate students in the Department of Chemistry, The University of Western Ontario. PB and Titiksha acknowledge a MITACS-Globalink funded internship in the Consta lab. S.C. acknowledges an NSERC-Discovery grant (Canada) for funding this research. V.K. acknowledges the Province of Ontario and The University of Western Ontario for the Queen Elizabeth II Graduate Scholarship in Science and Technology. Digital Research Alliance of Canada is acknowledged for providing the computing facilities.

References

- (1) Consta, S.; Oh, M. I.; Malevanets, A. New mechanisms of macroion-induced disintegration of charged droplets. *Chem. Phys. Lett.* **2016**, *663*, 1–12.
- (2) Kirkwood, J. G.; Shumaker, J. B. Forces between protein molecules in solution arising from fluctuations in proton charge and configuration. *Proc. Natl. Acad. Sci. U.S.A.* **1952**, *38*, 863–871.
- (3) Oosawa, F. *Polyelectrolytes*; Marcel Dekker Inc., New York, 1971.
- (4) Taylor, G. Disintegration of water drops in an electric field. *Proc. R. Soc. Lond. A* **1964**, *280*, 383–397.

- (5) Fernandez de la Mora, J. The fluid dynamics of Taylor cones. *Annu. Rev. Fluid Mech.* **2007**, *39*, 217–243.
- (6) Consta, S. Atomistic modeling of jet formation in charged droplets. *J. Phys. Chem. B* **2022**, *126*, 8350–8357.
- (7) Constantopoulos, T. L.; Jackson, G. S.; Enke, C. G. Effects of salt concentration on analyte response using electrospray ionization mass spectrometry. *J. Am. Soc. Mass Spectrom.* **1999**, *10*, 625–634.
- (8) Enke, C. G. A predictive model for matrix and analyte effects in electrospray ionization of singly-charged ionic analytes. *Anal. Chem.* **1997**, *69*, 4885–4893.
- (9) Kwan, V.; Consta, S. Bridging electrostatic properties between nanoscopic and microscopic highly charged droplets. *Chem. Phys. Lett.* **2020**, *746*, 137238.
- (10) Kwan, V.; Consta, S. Molecular characterization of the surface excess charge layer in droplets. *J. Am. Soc. Mass. Spectrom.* **2020**, *32*, 33–45.
- (11) Kwan, V.; O’Dwyer, R.; Laur, D.; Tan, J.; Consta, S. Relation between ejection mechanism and ion abundance in the electric double layer of droplets. *J. Phys. Chem. A* **2021**, *125*, 2954–2966.
- (12) Dole, M.; Mack, L.; Hines, R.; Mobley, R.; Ferguson, L.; Alice, M. d. Molecular beams of macroions. *J. Chem. Phys.* **1968**, *49*, 2240–2249.
- (13) Mack, L. L.; Kralik, P.; Rheude, A.; Dole, M. Molecular beams of macroions. II. *J. Chem. Phys.* **1970**, *52*, 4977–4986.
- (14) Fenn, J. B. Ion formation from charged droplets: roles of geometry, energy, and time. *J. Am. Soc. Mass. Spectrom.* **1993**, *4*, 524–535.
- (15) de la Mora, J. F. Electrospray ionization of large multiply charged species proceeds via Dole’s charged residue mechanism. *Anal. Chim. Acta* **2000**, *406*, 93–104.
- (16) Loscertales, I.; Fernández De La Mora, J. Experiments on the kinetics of field evaporation of small ions from droplets. *J. Chem. Phys.* **1995**, *103*, 5041–5060.
- (17) Karas, M.; Hillenkamp, F. Laser desorption ionization of proteins with molecular masses exceeding 10,000 daltons. *Anal. Chem.* **1988**, *60*, 2299–2301.
- (18) Trimpin, S.; Lu, I.-C.; Rauschenbach, S.; Hoang, K.; Wang, B.; Chubatyi, N. D.; Zhang, W.-J.; Inutan, E. D.; Pophristic, M.; Sidorenko, A. et al. Spontaneous charge separation and sublimation processes are ubiquitous in nature and in ionization processes in mass spectrometry. *J. Am. Soc. Mass. Spectrom.* **2017**, *29*, 304–315.
- (19) Trimpin, S.; Pophristic, M.; Adeniji-Adele, A.; Tomsho, J. W.; McEwen, C. N. Vacuum matrix-assisted ionization source offering simplicity, sensitivity, and exceptional robustness in mass spectrometry. *Anal. Chem.* **2018**, *90*, 11188–11192.
- (20) Apsokardu, M. J.; Kerecman, D. E.; Johnston, M. V. Ion formation in droplet-assisted ionization. *Rapid Communications in Mass Spectrometry* **2021**, *35*, e8227.
- (21) Pervukhin, V. V.; Sheven, D. G. Aerodynamic thermal breakup droplet ionization in mass spectrometric drug analysis. *Journal of the American Society for Mass Spectrometry* **2020**, *31*, 1074–1082.
- (22) Martini, P.; Albertini, S.; Laimer, F.; Meyer, M.; Gatchell, M.; Echt, O.; Zappa, F.; Scheier, P. Splashing of large helium nanodroplets upon surface collisions. *Phys. Rev. Lett.* **2021**, *127*, 263401.
- (23) Qin, Y.; Wingen, L.; Finlayson-Pitts, B. Toward a molecular understanding of the surface composition of atmospherically relevant organic particles. *Proc.*

- Natl. Acad. Sci. U.S.A.* **2022**, *119*, e2209134119.
- (24) Grimm, R. L.; Beauchamp, J. Evaporation and discharge dynamics of highly charged multicomponent droplets generated by electrospray ionization. *J. Phys. Chem. A* **2009**, *114*, 1411–1419.
- (25) Smith, J. N.; Flagan, R. C.; Beauchamp, J. Droplet evaporation and discharge dynamics in electrospray ionization. *J. Phys. Chem. A* **2002**, *106*, 9957–9967.
- (26) Upton, K. T.; Schilling, K. A.; Beauchamp, J. Easily fabricated ion source for characterizing mixtures of organic compounds by direct analysis in real time mass spectrometry. *Analytical Methods* **2017**, *9*, 5065–5074.
- (27) Jarrold, M. F. Applications of charge detection mass spectrometry in molecular biology and biotechnology. *Chem. Rev.* **2021**, *122*, 7415–7441.
- (28) Hirabayashi, A.; Sakairi, M.; Koizumi, H. Sonic spray ionization method for atmospheric pressure ionization mass spectrometry. *Anal. Chem.* **1994**, *66*, 4557–4559.
- (29) Blakley, C.; Vestal, M. Thermospray interface for liquid chromatography/mass spectrometry. *Anal. Chem.* **1983**, *55*, 750–754.
- (30) Wong, S. F.; Meng, C. K.; Fenn, J. B. Multiple charging in electrospray ionization of poly(ethylene glycols). *J. Chem. Phys.* **1988**, *92*, 546–550.
- (31) Ingram, A. J.; Boeser, C. L.; Zare, R. N. Going beyond electrospray: mass spectrometric studies of chemical reactions in and on liquids. *Chem. Sci.* **2016**, *7*, 39–55.
- (32) Wei, Z.; Li, Y.; Cooks, R. G.; Yan, X. Accelerated reaction kinetics in microdroplets: Overview and recent developments. *Annu. Rev. Phys. Chem.* **2020**, *71*, 31–51.
- (33) Fenn, J. B.; Rosell, J.; Meng, C. K. In electrospray ionization, how much pull does an ion need to escape its droplet prison? *J. Am. Soc. Mass. Spectrom.* **1997**, *8*, 1147–1157.
- (34) Consta, S.; Chung, J. K. Charge-induced conformational changes of PEG-(Na(n)(+)) in a vacuum and aqueous nanodroplets. *J. Phys. Chem. B* **2011**, *115*, 10447–10455.
- (35) Consta, S.; Malevanets, A. Manifestations of Charge Induced Instability in Droplets Effected by Charged Macromolecules. *Phys. Rev. Lett.* **2012**, *109*, 148301.
- (36) Chremos, A.; Douglas, J. F. Counterion distribution around flexible polyelectrolytes having different molecular architecture. *Soft Matter* **2016**, *12*, 2932–2941.
- (37) Dobrynin, A. V.; Rubinstein, M. Theory of polyelectrolytes in solutions and at surfaces. *Progress in Polymer Science* **2005**, *30*, 1049–1118.
- (38) Wilm, M. Principles of electrospray ionization. *Mol. Cell. Proteomics* **2011**, *10*, M111–009407.
- (39) Rayleigh, L. XX. On the equilibrium of liquid conducting masses charged with electricity. *Philos. Mag.* **1882**, *14*, 184–186.
- (40) Hendricks, C.; Schneider, J. Stability of a conducting droplet under the influence of surface tension and electrostatic forces. *Am. J. Phys.* **1963**, *31*, 450–453.
- (41) Peters, J. Rayleigh’s electrified water drops. *European Journal of Physics* **1980**, *1*, 143.
- (42) Consta, S.; Malevanets, A. Disintegration mechanisms of charged nanodroplets: novel systems for applying methods of activated processes. *Molec. Simul.* **2015**, *41*, 73–85.

- (43) Oh, M. I.; Malevanets, A.; Paliy, M.; Frenkel, D.; Consta, S. When droplets become stars: charged dielectric droplets beyond the Rayleigh limit. *Soft Matter* **2017**, *13*, 8781–8795.
- (44) Gomez, A.; Tang, K. Charge and fission of droplets in electrostatic sprays. *Phys. Fluids* **1994**, *6*, 404–414.
- (45) Duft, D.; Achtzehn, T.; Muller, R.; Huber, B. A.; Leisner, T. Coulomb fission: Rayleigh jets from levitated microdroplets. *Nature* **2003**, *421*, 128–128.
- (46) Malevanets, A.; Consta, S. Variation of droplet acidity during evaporation. *J. Chem. Phys.* **2013**, *138*, 184312.
- (47) Chamberlayne, C. F.; Zare, R. N. Simple model for the electric field and spatial distribution of ions in a microdroplet. *J. Chem. Phys.* **2020**, *152*, 184702.
- (48) Consta, S. Manifestation of Rayleigh instability in droplets containing multiply charged macroions. *J. Phys. Chem. B* **2010**, *114*, 5263–5268.
- (49) Chung, J. K.; Consta, S. Release mechanisms of poly(ethylene glycol) macroions from aqueous charged nanodroplets. *J. Phys. Chem. B* **2012**, *116*, 5777–5785.
- (50) Soltani, S.; Oh, M. I.; Consta, S. Effect of solvent on the charging mechanisms of poly (ethylene glycol) in droplets. *J. Chem. Phys.* **2015**, *142*, 114307.
- (51) Kebarle, P.; Tang, L. From ions in solution to ions in the gas phase—the mechanism of electrospray mass spectrometry. *Anal. Chem.* **1993**, *65*, 972A–986A.
- (52) Iribarne, J. V.; Thomson, B. A. On the evaporation of small ions from charged droplets. *J. Chem. Phys.* **1976**, *64*, 2287–2294.
- (53) Thomson, B.; Iribarne, J. Field induced ion evaporation from liquid surfaces at atmospheric pressure. *J. Chem. Phys.* **1979**, *71*, 4451–4463.
- (54) Kwan, V.; Consta, S. Conical Shape Fluctuations Determine the Rate of Ion Evaporation and the Emitted Cluster Size Distribution from Multicharged Droplets. *J. Phys. Chem. A* **2022**,
- (55) Kebarle, P. A brief overview of the present status of the mechanisms involved in electrospray mass spectrometry. *J. Mass Spectrom.* **2000**, *35*, 804–817.
- (56) Nguyen, S.; Fenn, J. B. Gas-phase ions of solute species from charged droplets of solutions. *Proc. Natl. Acad. Sci. U.S.A.* **2007**, *104*, 1111–1117.
- (57) Oh, M. I.; Consta, S. Charging and Release Mechanisms of Flexible Macromolecules in Droplets. *J. Am. Soc. Mass. Spectrom.* **2017**, *28*, 2262–2279.
- (58) Oh, M. I. Computational and analytical modelling of droplet-macroion interactions. Ph.D. thesis, The University of Western Ontario, 2018.
- (59) Zapletal, V.; Mládek, A.; Melková, K.; Louša, P.; Nomilner, E.; Jaseňáková, Z.; Kubáň, V.; Makovická, M.; Laníková, A.; Židek, L. et al. Choice of Force Field for Proteins Containing Structured and Intrinsically Disordered Regions. *Biophys. J.* **2020**, *118*, 1621–1633.
- (60) Konermann, L.; Ahadi, E.; Rodriguez, A. D.; Vahidi, S. Unraveling the mechanism of electrospray ionization. *Anal. Chem.* **2013**, *85*, 2–9.
- (61) Konermann, L.; Rodriguez, A. D.; Liu, J. On the formation of highly charged gaseous ions from unfolded proteins by Electrospray Ionization. *Anal. Chem.* **2012**, *84*, 6798–6804.
- (62) Soleilhac, A.; Dagany, X.; Dugourd, P.; Girod, M.; Antoine, R. Correlating droplet size with temperature changes in electrospray source by optical methods. *Anal. Chem.* **2015**, *87*, 8210–8217.

- (63) Gibson, S. C.; Feigerle, C. S.; Cook, K. D. Fluorometric measurement and modeling of droplet temperature changes in an electrospray plume. *Anal. Chem.* **2013**, *86*, 464–472.
- (64) Phillips, J. C.; Braun, R.; Wang, W.; Gumbart, J.; Tajkhorshid, E.; Villa, E.; Chipot, C.; Skeel, R. D.; Kalé, L.; Schulten, K. Scalable molecular dynamics with NAMD. *J. Comput. Chem.* **2005**, *26*, 1781–1802.
- (65) Hess, B.; Kutzner, C.; van der Spoel, D.; Lindahl, E. GROMACS 4: Algorithms for Highly Efficient, Load-Balanced, and Scalable Molecular Simulation. *J. Chem. Theory Comput.* **2008**, *4*, 435–447.
- (66) Berendsen, H. J.; van der Spoel, D.; van Drunen, R. GROMACS: a message-passing parallel molecular dynamics implementation. *Comput. Phys. Commun.* **1995**, *91*, 43–56.
- (67) Abraham, M. J.; Murtola, T.; Schulz, R.; Páll, S.; Smith, J. C.; Hess, B.; Lindahl, E. GROMACS: High performance molecular simulations through multi-level parallelism from laptops to supercomputers. *SoftwareX* **2015**, *1*, 19–25.
- (68) Humphrey, W.; Dalke, A.; Schulten, K. VMD: Visual Molecular Dynamics. *J. Mol. Graphics* **1996**, *14*, 33–38.
- (69) Choi, Y. K.; Park, S.-J.; Park, S.; Kim, S.; Kern, N. R.; Lee, J.; Im, W. CHARMM-GUI polymer builder for modeling and simulation of synthetic polymers. *J. Chem. Theory Comput.* **2021**, *17*, 2431–2443.
- (70) Jo, S.; Kim, T.; Iyer, V. G.; Im, W. CHARMM-GUI: A web-based graphical user interface for CHARMM. *Journal of Computational Chemistry* **2008**, *29*, 1859–1865.
- (71) Lee, J.; Cheng, X.; Swails, J. M.; Yeom, M. S.; Eastman, P. K.; Lemkul, J. A.; Wei, S.; Buckner, J.; Jeong, J. C.; Qi, Y. et al. CHARMM-GUI input generator for NAMD, GROMACS, AMBER, openmm, and charmm/openmm simulations using the CHARMM36 additive force field. *J. Chem. Theory Comput.* **2015**, *12*, 405–413.
- (72) Vega, C.; de Miguel, E. Surface tension of the most popular models of water by using the test-area simulation method. *J. Chem. Phys.* **2007**, *126*, 154707.
- (73) Chen, F.; Smith, P. E. Simulated surface tensions of common water models. *J. Chem. Phys.* **2007**, *126*, 221101.
- (74) Watson, H. C. The Stereochemistry of the Protein Myoglobin. *Prog. Stereochem.* **1969**, *4*, 299–333.
- (75) Metwally, H.; Duez, Q.; Konermann, L. Chain ejection model for electrospray ionization of unfolded proteins: evidence from atomistic simulations and ion mobility spectrometry. *Anal. Chem.* **2018**, *90*, 10069–10077.
- (76) Maurus, R.; Overall, C. M.; Bogumil, R.; Luo, Y.; Mauk, A.; Smith, M.; Brayer, G. D. A myoglobin variant with a polar substitution in a conserved hydrophobic cluster in the heme binding pocket. *Biochimica et Biophysica Acta (BBA) - Protein Structure and Molecular Enzymology* **1997**, *1341*, 1–13.
- (77) Huang, J.; Rauscher, S.; Nawrocki, G.; Ran, T.; Feig, M.; de Groot, B. L.; Grubmüller, H.; MacKerell, A. D., Jr CHARMM36m: an improved force field for folded and intrinsically disordered proteins. *Nat. Methods* **2017**, *14*, 71–73.
- (78) Abascal, J. L. F.; Vega, C. A general purpose model for the condensed phases of water: TIP4P/2005. *J. Chem. Phys.* **2005**, *123*, 234505.
- (79) Sharawy, M.; Consta, S. Effect of counterions on the charging mechanisms of a macromolecule in aqueous nanodrops. *J. Chem. Phys.* **2014**, *141*, 104321.

- (80) Glaeser, R. M. Proteins, interfaces, and cryo-EM grids. *Current Opinion in Colloid & Interface Science* **2018**, *34*, 1–8, Microscopy Methods: You Can Observe a Lot by Watching.